J|A|C|S ARTICLES

Published on Web 08/11/2010

Energetic and Entropic Contributions to Self-Assembly of Binary Nanocrystal Superlattices: Temperature as the Structure-Directing Factor

Maryna I. Bodnarchuk,[†,§] Maksym V. Kovalenko,[†] Wolfgang Heiss,[‡] and Dmitri V. Talapin*[,†]

Department of Chemistry and James Franck Institute, University of Chicago, Chicago, Illinois 60637, and Institute of Semiconductor and Solid State Physics, Johannes Kepler University Linz, A-4040 Linz, Austria

Received April 12, 2010; E-mail: dvtalapin@uchicago.edu

Abstract: We studied the effect of temperature on self-assembly of monodisperse colloidal nanocrystals into single-component and binary superlattices. Temperature, which serves as a weighting factor for the internal energy (U) and entropy (S) contributions to the Helmholtz free energy $F = U - TS$, allows tailoring relative weights of the interparticle interactions and free-volume entropy during the formation of nanocrystal superlattices. Temperature also provides a convenient tool for directing self-assembly of nanocrystals toward desired superlattice structures. We found that temperature strongly affects the structures of binary superlattices self-assembled from the mixtures of CdSe + PbS nanocrystals and PbSe + Pd nanocrystals. In the former case, small Hamaker constants for CdSe and PbS nanocrystals led to a relatively simple phase diagram, including only high-density $NaZn_{13}$-, AlB_2-, and NaCl-type binary superlattices. In contrast, binary superlattices self-assembled at different temperatures from PbSe and Pd nanocrystals showed a number of low-density complex phases stabilized by strong local van der Waals interactions between Pd nanocrystals. The structural diversity of nanoparticle superlattices is shown to be a result of the cooperative effect of the entropy-driven crystallization and the interparticle interactions. Both ΔU and $T\Delta S$ terms associated with the superlattice formation should be of the same order of magnitude, with $|\Delta U| < |T\Delta S|$ for the assembly of CdSe and PbS nanocrystals and $|\Delta U| > |T\Delta S|$ for the PbSe and Pd nanocrystals.

1. Introduction

One of the most fascinating directions in contemporary materials research is the use of precisely engineered molecules and nanostructures as the building blocks for hierarchical self-assembly of functional materials and devices.[1−4] Among such materials, the long-range ordered arrays of colloidal nanocrystals (NCs) attract steadily growing fundamental and practical interest. Owing to excellent size and shape uniformity, NCs can spontaneously order into single-component superlattices (SLs)[5−7] and binary nanocrystal superlattices (BNSLs)[1,8−13] upon evaporation of concentrated colloidal solutions. It is anticipated that the rationally engineered NC assemblies will provide novel opportunities for electronic,[14,15] optoelectronic,[16] thermoelectric,[17] catalytic, and other applications. Progress in the development of practical materials from NCs will require controllable growth of SLs with desired structures and morphologies and should rely on a deep understanding of the physics and chemistry of NC self-assembly.

The formation of single-component NC SLs is rather well understood[5,18−20] and can be controllably achieved for different

[†] University of Chicago.
[‡] Johannes Kepler University Linz.
[§] On leave from Johannes Kepler University Linz.

(1) Redl, F. X.; Cho, K. S.; Murray, C. B.; O'Brien, S. *Nature* **2003**, *423*, 968–971.
(2) Yaghi, O. M.; O'Keeffe, M.; Ockwig, N. W.; Chae, H. K.; Eddaoudi, M.; Kim, J. *Nature* **2003**, *423*, 705–714.
(3) Trikalitis, P. N.; Rangan, K. K.; Bakas, T.; Kanatzidis, M. G. *Nature* **2001**, *410*, 671–675.
(4) Mirkin, C. A.; Letsinger, R. L.; Mucic, R. C.; Storhoff, J. J. *Nature* **1996**, *382*, 607–609.
(5) Murray, C. B.; Kagan, C. R.; Bawendi, M. G. *Annu. Rev. Mater. Sci.* **2000**, *30*, 545–610.
(6) Li, L.-S.; Walda, J.; Manna, L.; Alivisatos, A. P. *Nano Lett.* **2002**, *2*, 557–560.
(7) Kiely, C. J.; Fink, J.; Brust, M.; Bethel, D.; Schiffrin, D. J. *Nature* **1998**, *396*, 444–446.
(8) Cheon, J.; Park, J. I.; Choi, J. S.; Jun, Y. W.; Kim, S.; Kim, M. G.; Kim, Y. M.; Kim, Y. J. *Proc. Natl. Acad. Sci. U.S.A.* **2006**, *103*, 3023–3027.
(9) Chen, Z.; O'Brien, S. *ACS Nano* **2008**, *2*, 1219–1229.
(10) Shevchenko, E. V.; Talapin, D. V.; Kotov, N. A.; O'Brien, S.; Murray, C. B. *Nature* **2006**, *439*, 55–59.
(11) Overgaag, K.; Evers, W.; de Nijs, B.; Koole, R.; Meeldijk, J.; Vanmaekelbergh, D. *J. Am. Chem. Soc.* **2008**, *130*, 7833–7835.
(12) Smith, D. K.; Goodfellow, B.; Smilgies, D.-M.; Korgel, B. A. *J. Am. Chem. Soc.* **2009**, *131*, 3281–3290.
(13) Shevchenko, E. V.; Kortright, J. B.; Talapin, D. V.; Aloni, S.; Alivisatos, A. P. *Adv. Mater.* **2007**, *19*, 4183–4187.
(14) Talapin, D. V.; Murray, C. B. *Science* **2005**, *310*, 86–89.
(15) Urban, J. J.; Talapin, D. V.; Shevchenko, E. V.; Kagan, C. R.; Murray, C. B. *Nat. Mater.* **2007**, *6*, 115–121.
(16) Konstantatos, G.; Howard, I.; Fischer, A.; Hoogland, S.; Clifford, J.; Klem, E.; Levina, L.; Sargent, E. H. *Nature* **2006**, *442*, 180–183.
(17) Harman, T. C.; Taylor, P. J.; Walsh, M. P.; LaForge, B. E. *Science* **2002**, *297*, 2229–2232.

materials. At the same time, previous studies have demonstrated that co-assembly of two types of NCs can yield BNSLs exhibiting very rich phase diagrams with multiple close-packed and non-close-packed periodic[10,21] and even aperiodic quasicrystalline phases.[22] Recently, Vanmaekelbergh's group has reported self-assembly of ternary nanoparticle superlattices.[23] At the same time, little is known about the driving forces for BNSL formation. So far, most experimental studies used highly empirical and serendipitous choices of experimental conditions for BNSL growth and did not provide a thorough assessment of thermodynamic and kinetic factors contributing to the NC assembly process.

From a thermodynamics perspective, the problem of finding the equilibrium configuration for a large ensemble of particles can be treated as minimization of the Helmholtz free energy (F).[24,25] For a closed system F is generally expressed through the internal energy (U), entropy (S), and temperature (T):

$$F = U - TS \quad (1)$$

The contributions to the free energy of the equilibrium ensemble can be subdivided into energetic and entropic. The internal energy is determined by specific interactions between NCs, which can interact with each other in a very complex manner, just like atoms in metallic,[26] ionic, or molecular crystals.[27,28] Experimental studies of various NC systems have revealed Coulombic,[10,29] dipole−dipole,[30] and van der Waals (vdW)[31] interactions between NC inorganic cores. Furthemore, the hydrocarbon tails of the NC ligand molecules can interact with each other, generating either attractive or repulsive forces, depending on solvent and interparticle distance.[32] The entropy changes during the self-assembly process are generally related to the vibrational and configurational degrees of freedom,[5,33] as will be discussed below.

Thermodynamics of sphere packing is an active research field, with numerous theoretical and experimental studies outlining the effects of entropy,[34−38] interparticle potentials,[29,39−43] and polydispersity[44,45] on nucleation and growth of ordered phases. To apply existing theoretical framework to real NCs, we need quantitative estimates for all terms contributing to U and S in eq 1. Unfortunately, there is no current agreement on the hierarchy of the energy scales acting during self-assembly of NCs into BNSLs. Enormous structural diversity and observation of non-close-packed BNSL phases suggest the important role of specific pair potentials.[10] Simple estimations predict that the strengths of Coulombic, dipolar, and vdW forces between individual NCs should be of the same order of magnitude,[46] further complicating theoretical analysis of BNSL phase diagrams. On the other hand, Chen and O'Brien recently studied self-assembly of CdSe and CdTe NCs and proposed that the formation of BNSL from these NCs was mainly driven by free volume entropy, leading to the structures with the highest packing density for a given particle size ratio.[9] Their observations of CdTe−CdTe BNSLs isostructural with AlB_2, $NaZn_{13}$, $CaCu_5$, and $MgZn_2$ intermetallic compounds have been rationalized on the basis of simple space-filling principles, long known for colloidal hard spheres.[5,33]

In this work we report an experimental study of the effect of temperature on the formation of single-component and binary NC superlattices. According to eq 1, temperature can be used as the weighting factor for the energetic and entropic contributions. The role of entropy can be effectively increased by increasing the temperature while keeping all other parameters constant, thus offering a tool for predictable screening of BNSL phase diagrams and for guiding the NC self-assembly toward desired structures.

2. Experimental Section

2.1. Nanocrystal Synthesis. PbSe NCs stabilized with oleic acid were synthesized from lead oleate and TOPSe. The details of preparation can be found in ref 14. Synthesis of PbS NCs capped with oleic acid was performed from lead oleate and bis(trimethylsilyl)sulfide according to ref 47. CdSe NCs were synthesized according to ref 48 from dimethylcadmium and TOPSe in a mixture of hexadecylamine, trioctylphosphine oxide, and trioctylphosphine. The synthesis of $Fe_xO/CoFe_2O_4$ core−shell NCs was carried out by high-temperature decomposition of mixed iron(III)/cobalt(II) oleate at 320 °C in the presence of oleic acid as the stabilizing agent.[49] Dodecanethiol-stabilized 3.4 and 4.9 nm Pd NCs were synthesized as described in ref 10. Palladium acetate was used instead of palladium chloride as precursor for synthesis of 4.9 nm Pd NCs, and the reaction was carried out at 60 °C.

(18) Bigioni, T. P.; Lin, X. M.; Nguyen, T. T.; Corwin, E. I.; Witten, T. A.; Jaeger, H. M. *Nat. Mater.* **2006**, *5*, 265–270.
(19) Pileni, M. P. *J. Phys. Chem. B* **2001**, *105*, 3358–3371.
(20) Rupich, S. M.; Shevchenko, E. V.; Bodnarchuk, M. I.; Lee, B.; Talapin, D. V. *J. Am. Chem. Soc.* **2010**, *132*, 289–296.
(21) Shevchenko, E. V.; Talapin, D. V.; Murray, C. B.; O'Brien, S. *J. Am. Chem. Soc.* **2006**, *128*, 3620–3637.
(22) Talapin, D. V.; Shevchenko, E. V.; Bodnarchuk, M. I.; Ye, X. C.; Chen, J.; Murray, C. B. *Nature* **2009**, *461*, 964–967.
(23) Evers, W. H.; Friedrich, H.; Filion, L.; Dijkstra, M.; Vanmaekelbergh, D. *Angew. Chem., Int. Ed.* **2009**, *48*, 9655–9657.
(24) Frenkel, D.; Mulder, B. M.; McTague, J. P. *Phys. Rev. Lett.* **1984**, *52*, 287–290.
(25) Eldridge, M. D.; Madden, P. A.; Frenkel, D. *Mol. Phys.* **1993**, *79*, 105–120.
(26) Shoemaker, D. P.; Marsh, R. E.; Ewing, F. J.; Pauling, L. *Acta Crystallogr.* **1952**, *5*, 637–644.
(27) Barrat, J. L.; Vos, W. L. *J. Chem. Phys.* **1992**, *97*, 5707–5712.
(28) Loubeyre, P.; Jeanlouis, M.; Letoullec, R.; Charongerard, L. *Phys. Rev. Lett.* **1993**, *70*, 178–181.
(29) Kalsin, A. M.; Fialkowski, M.; Paszewski, M.; Smoukov, S. K.; Bishop, K. J. M.; Grzybowski, B. A. *Science* **2006**, *312*, 420–424.
(30) Lalatonne, Y.; Richardi, J.; Pileni, M. P. *Nat. Mater.* **2004**, *3*, 121–125.
(31) Ohara, P. C.; Leff, D. V.; Heath, J. R.; Gelbart, W. M. *Phys. Rev. Lett.* **1995**, *75*, 3466–3469.
(32) Schapotschnikow, P.; Pool, R.; Vlugt, T. J. H. *Nano Lett.* **2008**, *8*, 2930–2934.
(33) Murray, M. J.; Sanders, J. V. *Philos. Mag. A* **1980**, *42*, 721–740.
(34) Eldridge, M. D.; Madden, P. A.; Frenkel, D. *Nature* **1993**, *365*, 35–37.
(35) Bartlett, P.; Ottewill, R. H.; Pusey, P. N. *Phys. Rev. Lett.* **1992**, *68*, 3801–3804.
(36) Trizac, E.; Eldridge, M. D.; Madden, P. A. *Mol. Phys.* **1997**, *90*, 675–678.
(37) Cottin, X.; Monson, P. A. *J. Chem. Phys.* **1995**, *102*, 3354–3360.
(38) Hunt, N.; Jardine, R.; Bartlett, P. *Phys. Rev. E* **2000**, *62*, 900–913.
(39) Bishop, K. J. M.; Wilmer, C. E.; Soh, S.; Grzybowski, B. A. *Small* **2009**, *5*, 1600–1630.
(40) Min, Y.; Akbulut, M.; Kristiansen, K.; Golan, Y.; Israelachvili, J. *Nat. Mater.* **2008**, *7*, 527–538.
(41) Hynninen, A. P.; Christova, C. G.; van Roij, R.; van Blaaderen, A.; Dijkstra, M. *Phys. Rev. Lett.* **2006**, *96*, 138308.
(42) Hynninen, A. P.; Dijkstra, M. *Phys. Rev. Lett.* **2005**, *94*, 138303.
(43) Bartlett, P.; Campbell, A. I. *Phys. Rev. Lett.* **2005**, *95*, 128302.
(44) Auer, S.; Frenkel, D. *Nature* **2001**, *413*, 711–713.
(45) Pronk, S.; Frenkel, D. *J. Chem. Phys.* **2004**, *120*, 6764–6768.
(46) Talapin, D. V. *ACS Nano* **2008**, *2*, 1097–1100.
(47) Hines, M. A.; Scholes, G. D. *Adv. Mater.* **2003**, *15*, 1844–1849.
(48) Talapin, D. V.; Rogach, A. L.; Kornowski, A.; Haase, M.; Weller, H. *Nano Lett.* **2001**, *1*, 207–211.
(49) Bodnarchuk, M. I.; Kovalenko, M. V.; Groiss, H.; Resel, R.; Reissner, M.; Hesser, G.; Lechner, R. T.; Steiner, W.; Schäffler, F.; Heiss, W. *Small* **2009**, *5*, 2247–2252.

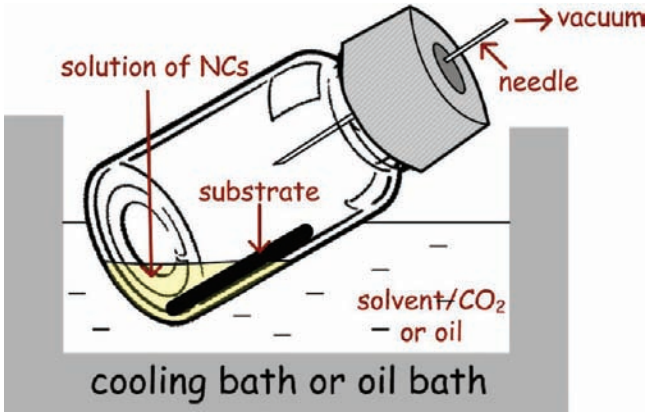

Figure 1. Setup used for studies of self-assembly of different nanocrystals into single-component and binary superlattices at various temperatures.

2.2. Preparation of Binary Superlattices at Different Temperatures. We used an experimental setup shown in Figure 1 to carry out self-assembly experiments in the temperature range between −60 and 120 °C. Carbon-coated copper TEM grids (type-B, Ted Pella) were used as the substrates for self-assembly experiments. The grids were dipped in toluene for 15 s to remove protective Formvar coating, followed by drying on filter paper. The grids were placed inside a tilted glass vial (∼60° tilt angle). Approximately 20 μL of solution containing a mixture of two types of NCs with the desired particle ratio was placed above the grid to cover it entirely. Concentrations of NCs were estimated either photometrically for CdSe, PbS, and PbSe using known extinction coefficients[50−52] or gravimetrically for all other NCs. In the latter case, the concentrations were corrected for ligand fraction known from thermogravimetric analysis of purified NC samples. Additional details are provided in the Supporting Information.[53] Various *n*-alkanes (octane, nonane, decane, undecane, dodecane, tetradecane, hexadecane, and octadecane) were used as solvents. The vials were placed in a cooling bath containing an organic solvent/dry ice mixture to obtain temperatures from −60 to −20 °C, in water/ice for 0 °C, or in an oil bath to reach 20−140 °C. The following cooling mixtures were used: tetrachloroethylene/dry ice for −20 °C, acetonitrile/dry ice for −40 °C, and isopropyl ether/dry ice for −60 °C. The solutions were evaporated under dynamic vacuum supplied via a needle penetrating the cap of the closed vial. The evaporation rate could be easily adjusted by using different gauge needles.

To maximize the reproducibility of self-assembly experiments, we carried out all temperature-dependent studies using the same batches of NCs for the entire temperature range. Each experiment was reproduced at least twice to ensure reproducibility of reported trends.

2.3. Structural Characterization of Nanocrystal Superlattices. Transmission electron microscopy (TEM) images and electron diffraction patterns were obtained using an FEI Technai F3 microscope operating at an acceleration voltage of 300 kV. The TEM images were compared to the BNSL projections simulated using Accelrys MS Modeling 4 and Crystal Maker 1.4 software packages. Small-angle electron diffraction (SAED) patterns measured over large BNSL areas were compared with the FFTs of real-space TEM images and with electron diffraction patterns simulated with Single Crystal 1.2.1 software.

In many cases, the comparison of experimental TEM images with two-dimensional (2D) projections of modeled crystal structures was sufficient for unambiguous structural assignments of BNSL structures. In several cases, however, this approach could lead to erroneous conclusions because of similarities in the BNSL projections of different structures. For example, the (100) projection of the AlB_2-type lattice (Figure S1a) appears similar to the (010) projection of the CuAu lattice (Figure S1b). To obtain information about three-dimensional (3D) packing of NCs in BNSLs, we complemented real-space TEM studies with the SAED patterns measured from BNSL domains. Compared to real-space images, SAED contains information about the 3D arrangement of NCs in the unit cell. Thus, similar real-space images shown in Figure S1a,b correspond to distinctly different electron diffraction patterns (Figure S1e,f) with different interplanar spacings ($1/d_{hkl}$). The ratios between different d_{hkl} values are uniquely defined by the lattice symmetry. On the basis of these ratios, we assigned the experimental electron diffraction in PbSe-Pd superlattices to the CuAu-type structure (Figure S1g). In some cases, Fourier transformation of TEM images can also provide useful information (Figure S1h,i).

In TEM tilting experiments, BNSL structures can be viewed at different angles with respect to the electron beam. This technique provides the most direct information about 3D arrangements of NCs in the unit cell.[54,55] We applied this technique to distinguish between (100) projections of AlB_2 structure and (010) projections of CuAu-type BNSLs (Figure S2). TEM tilting experiments were also employed to distinguish between (001) projections of CuAu and (001) projections of CsCl-type BNSLs (Figure S3) and to study a complex structure formed from 7.7 nm PbSe and 3.4 nm Pd NCs (Figure S4).

2.4. Measurements of Electrophoretic Mobility of Colloidal Nanocrystals. Measurements of electrophoretic mobility were performed using Zetasizer Nano-ZS (Malvern Instruments, Inc.). Colloidal solutions were tested using a dip-cell setup with Pd electrodes. Typical measurements of electrophoretic mobility included several scans of 100 runs each in the high-resolution mode. Dilution was optimized for each sample to achieve >100 kcps count rate and the best signal-to-noise ratio. The voltage applied to colloidal solutions was typically between 10 and 20 V.

3. Results and Discussion

3.1. Self-Assembly of Single-Component Nanoparticle Superlattices at Different Temperatures. Since we could not find any previous systematic studies related to the effect of temperature on self-assembly of NCs, we first studied how temperature affects the assembly of monodisperse NCs into single-component SLs. We used 11 nm $Fe_xO/CoFe_2O_4$ NCs,[49] which exhibited a strong tendency to self-assemble into superlattices[56] at different temperatures. Chloroform was used as a solvent providing good solubility for $Fe_xO/CoFe_2O_4$ NCs and suitable for the temperature range from −60 to +45 °C.

Both entropy and isotropic vdW interactions should favor the structures with highest packing density, namely face-centered cubic (fcc) and hexagonal close-packed (hcp).[57] In a hard-sphere system, fcc is favored over hcp due to its higher entropy, although the free energy difference is very small, about $10^{-3}k_BT$

(50) Yu, W. W.; Qu, L. H.; Guo, W. Z.; Peng, X. G. *Chem. Mater.* **2003**, *15*, 2854–2860.
(51) Cademartiri, L.; Montanari, E.; Calestani, G.; Migliori, A.; Guagliardi, A.; Ozin, G. A. *J. Am. Chem. Soc.* **2006**, *128*, 10337–10346.
(52) Moreels, I.; Lambert, K.; De Muynck, D.; Vanhaecke, F.; Poelman, D.; Martins, J. C.; Allan, G.; Hens, Z. *Chem. Mater.* **2007**, *19*, 6101–6106.
(53) For more details see Supporting information.
(54) Friedrich, H.; Gommes, C. J.; Overgaag, K.; Meeldijk, J. D.; Evers, W. H.; Nijs, B. d.; Boneschanscher, M. P.; de Jongh, P. E.; Verkleij, A. J.; de Jong, K. P.; van Blaaderen, A.; Vanmaekelbergh, D. *Nano Lett.* **2009**, *9*, 2719–2724.
(55) Chen, J.; Ye, X.; Murray, C. B. *ACS Nano* **2010**, *4*, 2374–2381.
(56) Bodnarchuk, M. I.; Kovalenko, M. V.; Pichler, S.; Fritz-Popovski, G.; Hesser, G. n.; Heiss, W. *ACS Nano* **2009**, *4*, 423–431.
(57) Talapin, D. V.; Shevchenko, E. V.; Murray, C. B.; Titov, A. V.; Kral, P. *Nano Lett.* **2007**, *7*, 1213–1219.

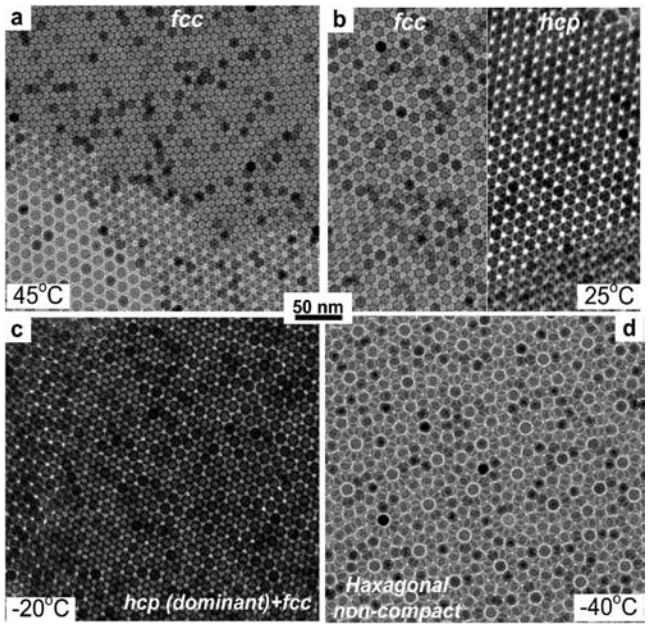

Figure 2. TEM images of superlattices self-assembled from chloroform solutions of 11 nm $Fe_xO/CoFe_2O_4$ nanocrystals at different temperatures: (a) face-centered cubic structure was formed at 45 °C; (b) face-centered cubic and hexagonal close-packed structures were formed at 25 °C; (c) hexagonal-close-packed structures were dominant at −20 °C; and (d) non-close-packed structures were formed at −40 °C.

per particle.[58] In addition, the solvent flow can direct NCs toward the fcc lattice.[59] In our case, the fcc structure formed almost exclusively at +45 °C (Figure 2a). When self-assembly of NCs was carried out at 25 °C, we observed the coexistence of hcp and fcc lattices (Figure 2b). Fcc and hcp structures could be easily distinguished in TEM images and electron diffraction patterns (Figure S5). At −20 °C the hcp structure became dominant (Figure 2c), with minor inclusions of non-close-packed (ncp) structures. The ncp hexagonal ordering was reproducibly observed in NC superlattices self-assembled at −40 °C (Figures 2d, S6, and S7).

The ncp structure shown in Figures 2d, S6, and S7 can be described as a stack of staggered hexagonally ordered layers rotated by an angle α with respect to each other. We modeled possible superlattice projections (Figures S6b) and found that the pattern with $\alpha = 30°$ is identical to that of the ncp structure self-assembled from 11 nm $Fe_xO/CoFe_2O_4$ NCs at −40 °C. Similar SLs have been previously reported for Au NCs.[60,61] To explain the formation of such low-density packing, Schiffrin et al. suggested that strong short-range electrostatic repulsion forced the NCs to occupy two-fold saddle points rather than three-fold hollow points above the underlying monolayer.[60] Similar structures with mutually rotated, hexagonally ordered 2D sheets have been observed for atomic layers in MoS_2,[62] for block-copolymer thin films,[63] and in DNA crystals.[64]

In addition to isotropic vdW forces between inorganic cores and organic ligands, magnetic NCs exhibit anisotropic dipolar magnetic interactions. As was previously reported,[49] $Fe_xO/CoFe_2O_4$ NCs possess rather small saturated magnetization of 15 emu/g (7.8×10^4 A/m), as compared to 90−100 emu/g (4.7×10^5−5.2×10^5 A/m) for bulk $CoFe_2O_4$[65] and 70−100 emu/g (3.7×10^5−5.2×10^5 A/m) for $CoFe_2O_4$ NCs of similar size.[66−68] This was attributed to the presence of an antiferromagnetic Fe_xO core and some disorder of surface spins. The role of magnetic interactions between NCs becomes progressively more important with lowering the temperature of the self-assembly process. The blocking temperature (T_B) measured by SQUID magnetometry for 11 nm NCs was 160 K, i.e., well below −40 °C (233 K) used in our self-assembly experiments. At the same time, T_B strongly depends on the experimental time scale. The mean time between two spin flips, also known as the Néel relaxation time (τ_N), is given by

$$\tau_N = \tau_0 \exp(KV/k_BT) \qquad (2)$$

where τ_0 is the attempt time, typically 10^{-9} s,[69] K is the magnetic anisotropy, and V is the NC volume. The time scale of SQUID measurement ($\tau_N = 100$ s) is very different from the time scales for adding of NCs to a growing superlattice. Recent in situ GISAXS studies[70] allow estimating that the appropriate time scale should lie in the millisecond domain. Without further speculations, we can obtain from eq 2 that, at this time scale, 11 nm $Fe_xO/CoFe_2O_4$ NCs with SQUID-measured $T_B = 160$ K should interact as ferromagnets up to temperatures as high as 290 K. The magnetic interaction energy (U_M) between two ferromagnetic NCs can be calculated as $U_M = (1/9)\pi\mu_0 R^3 M^2 \approx 3 \times 10^{-3}$ eV,[39] where μ_0 is the permeability of free space, R is the NC radius, and M is the magnetization. This value approaches $\sim 0.15 k_BT$ at −40 °C and is more than an order of magnitude larger than the interaction energy between fluctuating dipoles of two superparamagnetic NCs, known as the Kreesom interaction,[39] estimated as $\sim 10^{-5}$ eV. In a SL the magnetic dipoles of individual NCs are additionally stabilized by local dipole−dipole interactions.[71] On longer time scales the magnetization of a NC should switch between three mutually orthogonal (001)-type easy axes of $CoFe_2O_4$ phase. The local coupling of magnetic dipoles combined with dynamic switching of magnetization of individual NCs between several easy axes could be responsible for stabilization of the ncp structure shown in Figure 2d.

Theoretical studies of dipolar spheres have revealed that the energy of dipolar coupling (Madelung energy) for the hcp lattice

(58) Bolhuis, P. G.; Frenkel, D.; Mau, S. C.; Huse, D. A. *Nature* **1997**, *388*, 235–236.
(59) Norris, D. J.; Arlinghaus, E. J.; Meng, L.; Heiny, R.; Scriven, L. E. *Adv. Mater.* **2004**, *16*, 1393–1399.
(60) Fink, J.; Kiely, C. J.; Bethell, D.; Schiffrin, D. J. *Chem. Mater.* **1998**, *10*, 922–926.
(61) Zanchet, D.; Moreno, M. S.; Ugarte, D. *Phys. Rev. Lett.* **1999**, *82*, 5277.
(62) Reyes-Gasga, J.; Tehuacanero, S.; Yacaman, M. J. *Microsc. Res. Tech.* **1998**, *40*, 2–9.
(63) Luchnikov, V.; Kondyurin, A.; Formanek, P.; Lichte, H.; Stamm, M. *Nano Lett.* **2007**, *7*, 3628–3632.
(64) He, Y.; Ko, S. H.; Tian, Y.; Ribbe, A. E.; Mao, C. D. *Small* **2008**, *4*, 1329–1331.
(65) *Landolt-Bornstein*; Springer-Verlag: Berlin, 1983; Vol. 3−4.
(66) Song, Q.; Zhang, Z. J. *J. Am. Chem. Soc.* **2004**, *126*, 6164–6168.
(67) Lee, J. H.; Huh, Y. M.; Jun, Y.; Seo, J.; Jang, J.; Song, H. T.; Kim, S.; Cho, E. J.; Yoon, H. G.; Suh, J. S.; Cheon, J. *Nature Med.* **2007**, *13*, 95–99.
(68) Bao, N. Z.; Shen, L. M.; Padhan, P.; Gupta, A. *Appl. Phys. Lett.* **2008**, 92.
(69) McNab, T. K.; Fox, R. A.; Boyle, A. J. F. *J. Appl. Phys.* **1968**, *39*, 5703.
(70) Jiang, Z.; Lin, X.-M.; Sprung, M.; Narayanan, S.; Wang, J. *Nano Lett.* **2010**, *10*, 799–803.
(71) Murray, C. B.; Sun, S. H.; Doyle, H.; Betley, T. *MRS Bull.* **2001**, *26*, 985–991.

is higher than that for the fcc lattice.[72] The Madelung energy is proportional to m^2, where m is the particle magnetic moment. Upon increasing the strength of dipolar forces, phase transitions from fcc to hcp to base-centered orthorhombic and tetragonal (bco, bct) phases have been reported theoretically[42,73] and experimentally[74] in ensembles of spherical particles. The fcc structure should be more stable at high temperatures, while hcp should dominate at low temperatures. This is because the advantage that the hcp lattice gains from U in eq 1 is canceled at high T by the entropic term $-TS$.

Figure 2 shows that temperature can be a structure-directing factor in self-assembly of magnetic NCs. We also performed similar studies with nonmagnetic NCs (Au, Pd) and found a strong preference for the formation of fcc superlattices at all studied temperatures, as expected for crystallization of spherical particles with isotropic interparticle potentials.

3.2. Interparticle Interactions and Design of Experiments for Growing BNSLs. To date, all reported experiments on BNSL growth were carried out at 40−70 °C.[1,9,10,13,15,75−78] There are no obvious reasons for this choice other than NC solubility[21] and experimental convenience. Toluene or tetrachloroethylene was routinely used at these temperatures under ambient or reduced pressure. In the case of magnetic $Fe_xO/CoFe_2O_4$ NCs, we used chloroform as a solvent convenient for low temperatures. This approach, however, cannot provide acceptable accuracy for NCs interacting via electrostatic forces because of the strong temperature dependence of the static dielectric constants of common organic solvents. The other problem associated with using the same solvent for self-assembly of NCs at different temperatures is related to different solvent evaporation rates at different temperatures. We found no individual solvents suitable over a broad temperature range of −60 to 120 °C. At the same time, chemically different solvents can interact differently with NC surface ligands and thus alter the interparticle potentials.[79] To address all these problems, we carried out BNSL assembly in *n*-alkanes. The use of *n*-alkanes allowed us to vary the assembly temperature without significantly changing the solvent evaporation rate and dielectric constant, while providing similar chemical environments for a broad range of temperatures. We used a suitable *n*-alkane for each temperature point. For example, the equilibrium vapor pressures fall in the range of 0.5−0.6 Torr for hexane at −60 °C, heptane at −40 °C, octane at −20 °C, nonane at 0 °C, dodecane at 20 °C, tetradecane at 40 °C, hexadecane at 65 °C, and octadecane at 85−100 °C. The static dielectric constant (ε') of *n*-alkanes obeys the Clausius−Mossotti relation:[80]

$$(\varepsilon' - 1)/(\varepsilon' + 2) = 4\pi d N_A \alpha/3M_w \quad (3)$$

where ε' is the real part of the dielectric constant, d is the density, α is the polarizability of molecule, and M_w is the molecular weight. For *n*-alkanes, $\ln(1/d) = a/M_w - b$, where $\ln a = 0.00275T + 2.303$ and $b = 0.000182T^{1.19}$.[80] One can easily show that the ε' values for the above-described sequence of *n*-alkanes chosen as solvents for BNSL self-assembly lie in the narrow range of 1.99−2.04 due to the compensation of the higher dielectric constant for longer chain alkanes by the temperature effect on ε'. Available experimental data on ε' of *n*-alkanes fully confirm this trend.[81] Through similar "compensation" between M_w and thermal energy, the viscosity of the studied NC solutions remained nearly independent of temperature as well.[82] Chemical inertness is another important advantage of using *n*-alkanes as solvents.

In our experiments it took about 20−25 min to completely evaporate 25−30 μL of colloidal solution under mild vacuum. To maintain reproducible solvent vapor pressure inside the vials, we used the same gauge needles (Figure 1). In a series of reference experiments, we varied the needle gauge to tune the evaporation rate. The common result was that the type(s) of BNSL structure(s) and their approximate fractions remained independent of solvent evaporation rate. This led us to the conclusion that the assembly process occurs mostly under thermodynamic control.

The surface charge (Z in units of e) for a spherical particle in a low dielectric solvent can be estimated on the basis of the measured electrophoretic mobility:[83]

$$\mu_e = Ze/6\pi\eta R \quad (4)$$

where η is the solvent dynamic viscosity and R is the hydrodynamic radius. The ε' values of the *n*-alkanes used in this work (1.99−2.04)[80] were significantly lower than the ε' values of chlorinated (4.8 for chloroform at 25 °C) or aromatic (2.5 for toluene at 25 °C) solvents. Our electrophoretic mobility measurements showed that NCs possess considerable surface charge when dispersed in chloroform, whereas the low dielectric constants of *n*-alkanes reduced the effects of NC surface charging in nonpolar solvents.[10] For example, the population of charged 7.7 nm PbSe NCs in chloroform was significantly larger than in *n*-decane (Figure S8a,b). The electrophoretic mobility of 4.9 nm dodecanethiol-capped Pd NCs measured in *n*-decane at different temperatures did not reveal any charging of NCs. When corrected for temperature-dependent variations of solvent viscosity, μ_e of Pd NCs was found to be temperature-invariant (Figure S8c,d).

3.3. Remarks on Entropy and Packing Density. The packing density plays an important role in intermetallic compounds,[84] liquid crystals,[24] opals,[33,85] and NC superlattices.[9] The total entropy of an ideal gas of two types of particles (1:1 number ratio) is[86]

(72) Yethiraj, A.; Wouterse, A.; Groh, B.; van Blaaderen, A. *Phys. Rev. Lett.* **2004**, *92*, 058301.
(73) Brandt, P. C.; Ivlev, A. V.; Morfill, G. E. *J. Chem. Phys.* **2009**, *130*, 204513-9.
(74) Dassanayake, U.; Fraden, S.; van Blaaderen, A. *J. Chem. Phys.* **2000**, *112*, 3851–3858.
(75) Shevchenko, E. V.; Talapin, D. V.; Murray, C. B.; O'Brien, S. *J. Am. Chem. Soc.* **2006**, *128*, 3620–3637.
(76) Shevchenko, E. V.; Talapin, D. V.; O'Brien, S.; Murray, C. B. *J. Am. Chem. Soc.* **2005**, *127*, 8741–8747.
(77) Lu, C.; Chen, Z.; O'Brien, S. *Chem. Mater.* **2008**, *20*, 3594–3600.
(78) Overgaag, K.; Evers, W.; de Nijs, B.; Koole, R.; Meeldijk, J.; Vanmaekelbergh, D. *J. Am. Chem. Soc.* **2008**, *130*, 7833.
(79) Mattoussi, H.; Cumming, A. W.; Murray, C. B.; Bawendi, M. G.; Ober, R. *Phys. Rev. B* **1998**, *58*, 7850–7863.
(80) Sen, A. D.; Anicich, V. G.; Arakelian, T. *J. Phys. D-Appl. Phys.* **1992**, *25*, 516–521.
(81) Wohlfarth, C. *Landolt-Börnstein IV/17: Static Dielectric Constants of Pure Liquids and Binary Liquid Mixtures*; Springer-Verlag: Berlin Heidelberg, 2008.
(82) Knapstad, B.; Skjoelsvik, P. A.; Oeye, H. A. *J. Chem. Eng. Data* **1989**, *34*, 37–43.
(83) O'Brien, R. W.; White, L. R. *J. Chem. Soc., Faraday Trans.* **1978**, *74*, 1607–1626.
(84) Paszkowicz, W. *J. Phys. F: Met. Phys.* **1989**, *59*, 451–462.
(85) Sanders, J. V. *Philos. Mag. A* **1980**, *42*, 705–720.
(86) Angelani, L.; Foffi, G. *J. Phys.-Condens. Matter* **2007**, *19*, 256207.

$$S = \frac{5}{2}N - N\ln\left(\frac{N}{V}\right) - 3N\ln\lambda + \ln 2 \qquad (5)$$

where V is the volume, λ is the thermal de Broglie wavelength, and the term ln 2 accounts for the entropy of mixing. This formalism can be qualitatively applied to a NC solution. In general, S of an ordered array of spherical particles can be subdivided into configurational entropy and free volume entropy.[34,36,37] As solvent evaporates, the concentration of NCs increases and the free volume decreases. When the average interparticle distance becomes comparable to the particle dimensions, the system can undergo a transition from a disordered to an ordered state. The ordering reduces configurational entropy but leads to higher free volume entropy associated with the local free space available for each particle to perform translational and rotational movements. It has been shown that the gain in free volume entropy upon ordering of hard spheres can be larger than the decrease in configurational entropy, thus providing a net positive change in the system's entropy. This purely entropic effect forces the phase transition and stabilizes the ordered colloidal crystal state.[34,58]

The free volume entropy is related to the packing density of a SL. It is often asserted that the free volume per particle is inversely related to the packing fraction of a crystalline structure and that the entropy is proportional to the free volume.[87] In the absence of other significant forces, the ensemble of spheres should adopt a structure with the highest packing density. In the case of monodisperse particles, it will be fcc or hcp lattices with $\rho \approx 0.7405$, whereas in binary mixtures, the most favorable structure should be one with the highest density for a given particle size ratio $\gamma = d_{small}/d_{large}$. Space-filling curves plotting the space-filling factor (ρ) versus γ can be used to estimate relative entropic contributions to the change in free energy during the self-assembly process. Figure 3 shows calculated ρ vs γ curves for BNSL structures observed in this study (see Supporting Information for calculation details). Space-filling provides a good estimate for entropic contributions. At the same time, configurational entropy can help direct the assembly process between structures with similar ρ values. Thus, the slightly higher configurational entropy of the fcc lattice makes it more stable than hcp;[58] the higher configurational entropy of the aperiodic lattice compared to the periodic one stabilizes quasicrystalline NC superlattices.[22]

When ρ of a binary lattice exceeds that of a fcc structure, entropy alone can stabilize AB_n structure against phase separation into separately packed A and B components.[34] Accurate free energy calculations also predict that binary phases of hard spheres whose ρ is slightly below 0.7405 can be stabilized by additional configurational entropy and the entropy of mixing (eq 5).[88] Binary structures with $\rho < 0.7405$ can also be stabilized by interparticle interactions.[89] The conformational changes of surface ligands during formation of SLs should also provide an entropic contribution to the free energy of NC self-assembly. Little is known about the magnitude of this contribution.

3.4. Formation of BNSLs at Different Temperatures. In this study we used several fixed size ratios of small and large NCs ($\gamma_{eff} = d_{small}/d_{large}$) and studied how temperature affects BNSL formation at different relative concentrations of NCs. γ_{eff} was calculated using actual NC sizes estimated as $d_{NC} = d_{core} + 2d_{shell}$, where d_{shell} was the effective thickness of the ligand shells. Typically d_{shell} is smaller than the length of fully extended ligand molecules (e.g., 18 and 15.2 Å for oleic acid and 1-dodecanethiol, respectively), suggesting interpenetration of hydrocarbon tails of adjacent NCs.[90] NC size, material, and even sample preparation conditions can affect the packing density of surface ligand molecules. For example, successive washing of colloidal PbSe NCs partially removes oleic acid ligands attached to the NC surface, making the ligand shell effectively thinner. On the other hand, excessive washing often negatively affects the ability of NCs to self-assemble. In this work we measured d_{shell} as half the mean interparticle distance for single-component fcc SLs. This approach was used in previous works[75,91] and allows estimation of d_{shell} relevant to NC assembly. For NCs studied in this work, d_{shell} values were 1.1 nm for CdSe NCs synthesized in TDPA-HDA-TOPO-TOP mixture, 0.95 nm for oleic-acid-capped PbSe NCs, 0.85 nm for oleic-acid-capped PbS NCs, 0.85 nm for 3.4-nm dodecanethiol-capped Pd NCs, and 1.1 nm for 4.9-nm dodecanethiol-capped Pd NCs.

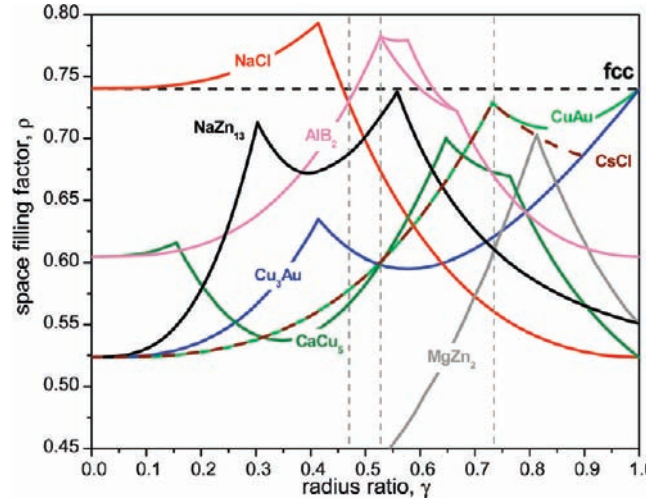

Figure 3. Calculated space-filling curves for NaCl, CsCl, CuAu, AlB_2, $MgZn_2$, Cu_3Au, $CaCu_5$, and $NaZn_{13}$ binary structures. Dashed vertical lines show γ_{eff} for nanocrystals studied in this work.

We studied self-assembly in three different NC systems: (i) 8.0 nm CdSe and 3.1 nm PbS NCs ($\gamma_{eff} = 0.47 \pm 0.02$), (ii) 7.7 nm PbSe and 3.4 nm Pd NCs ($\gamma_{eff} = 0.53 \pm 0.03$), and (iii) 7.7 nm PbSe and 4.9 nm Pd NCs ($\gamma_{eff} = 0.74 \pm 0.03$). The mean γ_{eff} values for the studied systems are shown in Figure 3 as vertical lines. The standard deviations for γ_{eff} were calculated for each system from experimentally measured NC size distributions. This choice of NCs was motivated by the availability of convenient synthetic routes toward monodisperse CdSe, PbSe, PbS, and Pd NCs. The Hamaker constants for metals interacting through a hydrocarbon layer are significantly larger than for metal chalcogenides,[92] and the vdW interactions between Pd NCs should be stronger than those between PbSe NCs. This difference originates from different dielectric responses of metals and dielectrics at the differerent optical

(87) Hynninen, A. P.; Filion, L.; Dijkstra, M. *J. Chem. Phys.* **2009**, *131*, 9.
(88) Xu, H.; Baus, M. *J. Phys. Condens. Matter* **1992**, *4*, L663–L668.
(89) Leunissen, M. E.; Christova, C. G.; Hynninen, A.-P.; Royall, C. P.; Campbell, A. I.; Imhof, A.; Dijkstra, M.; van Roij, R.; van Blaaderen, A. *Nature* **2005**, *437*, 235–240.
(90) Lee, B.; Podsiadlo, P.; Rupich, S.; Talapin, D. V.; Rajh, T.; Shevchenko, E. V. *J. Am. Chem. Soc.* **2009**, *131*, 16386–16388.
(91) Chen, Z.; Moore, J.; Radtke, G.; Sirringhaus, H.; O'Brien, S. *J. Am. Chem. Soc.* **2007**, *129*, 15702–15709.
(92) Bergström, L. *Adv. Colloid Interface Sci.* **1997**, *70*, 125–169.

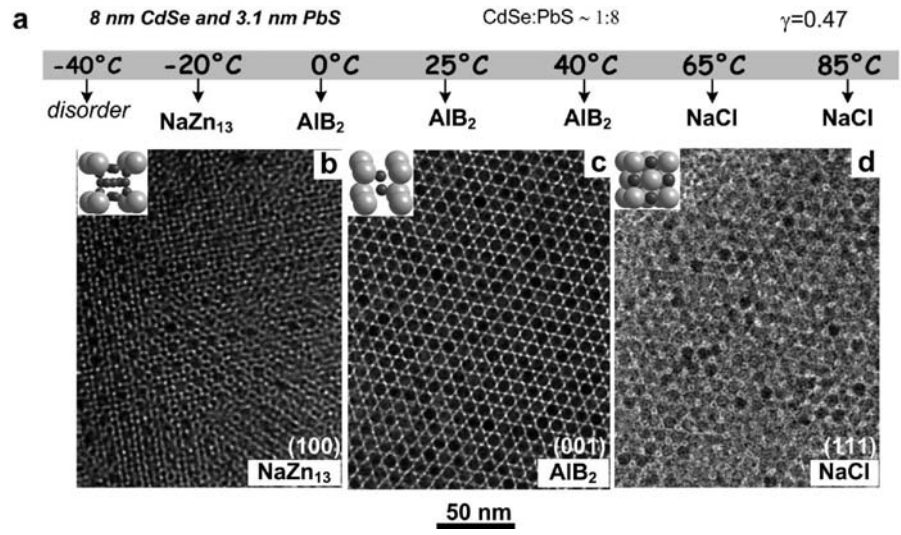

Figure 4. Self-assembly of 8 nm CdSe and 3.1 nm PbS nanocrystals at different temperatures. (a) Overview of the binary phases assembled at different temperatures. (b−d) Typical electron microscopy images of binary superlatices isostructural with (b) $NaZn_{13}$, (c) AlB_2, and (d) NaCl compounds.

frequencies.[93] Comparative studies of CdSe-PbS and PbSe-Pd NC systems allow the situations to be studied where the components have similar Hamaker constants, as in the former case, or show a large contrast in the strength of vdW forces, as in the latter case. Compared to Au and Ag, palladium NCs showed much better solubility in *n*-alkanes at low temperature, presumably because of denser coverage of the NC surface with dodecanethiol ligands. The choice of effective γ-ratios studied in this work was also justified by the availability of calculated phase diagrams for hard spheres at $\gamma = 0.45$,[37] 0.52 and 0.54,[94] and 0.72 and 0.74,[87,94] which allowed comparison of the behaviors of real NCs with the entropy-driven crystallization of hard spheres.

The only binary structure self-assembled at 85 °C from the mixtures of CdSe and PbS NCs was isostructural with NaCl (Figure 4a,d). At 65 °C, NaCl-type was the dominant binary structure, but we also observed the formation of small domains of AlB_2-type BNSLs, representing ~10−20% of all formed BNSL structures (Figure 4a,c). When the same NCs were mixed with the same concentrations but solvent was evaporated at 0, 25, or 40 °C, we reproducibly observed formation of AlB_2-type BNSLs. These two structures are the densest phases and have nearly identical packing densities of about 0.729 at $\gamma = 0.47$ (Figure 3). Further decrease of temperature led to the formation of $NaZn_{13}$-type lattice (Figure 4a,b) with much smaller calculated packing density (~0.658). The BNSLs shown in Figure 4 were all obtained from the solutions with ~1:8 concentration ratio for CdSe and PbS NCs. To adjust for the differences in NBSL stoichiometry, the NaCl- and AlB_2-type BNSLs coexisted on TEM grids with domains of fcc-packed PbS NCs. The samples with $NaZn_{13}$-type BNSLs also contained CdSe NCs in the form of either disordered or fcc-packed domains.

To explore a binary system of typical semiconductor and metal NCs, we studied co-assembly of PbSe and Pd NCs for two different particle size ratios ($\gamma_{eff} = 0.53$ and 0.74) at different temperatures and for different NC concentration ratios. Figure 3 shows that, at $\gamma = 0.53$, AlB_2 structure has its highest packing density ($\rho \approx 0.782$), significantly exceeding the packing density of the fcc lattice, and should be strongly favored by the free volume entropy. Rather surprisingly, the most common BNSL structures self-assembled from colloidal solutions of 7.7 nm PbSe NCs and 3.4 nm Pd NCs ($\gamma_{eff} \approx 0.53$) were not AlB_2-type but CuAu- and Cu_3Au-type BNSLs with packing fractions of only $\rho \approx 0.60$ (Figure 5a−c). Figure 5a shows BNSL phases assembled at different temperatures from solutions with 1:9 PbSe-to-Pd NC concentration ratio. Formation of CuAu and Cu_3Au structures was observed at −20, 40, 85, and 100 °C. At low temperature (−20 °C) these BNSLs co-existed with $NaZn_{13}$ (~20% of all formed BNSL domains) and AlB_2-type BNSLs (~35%). Near room temperature, the high-density AlB_2 phase (Figure 5f) dominated at all studied PbSe-to-Pd NC ratios. At 65 and 85 °C we observed reproducible formation of another binary phase (Figure 5h), resembling the Fe_4C lattice.[10] This structure was studied using TEM tilting experiments (Figure S4) and assigned to a BNSL with AB_4 stoichiometry, containing 32 small spheres and 8 large spheres per unit cell (Supporting Information). At 100 °C only CuAu and Cu_3Au BNSLs were observed. Table S1 in the Supporting Information compares the areas of TEM grids covered by different BNSL structures at each temperature.

When the concentration of Pd NCs was increased to ~1:18 PbSe-to-Pd NCs ratio, we observed a similar sequence of BNSL phases self-assembled at different temperatures (Figure 5b). The major difference compared to the 1:9 concentration ratio was the increased probability to form $NaZn_{13}$-type structures, which were the only BNSLs formed at −20 °C. $NaZn_{13}$ BNSLs were also observed at 25 °C (~20%) co-existing with AlB_2 and other BNSLs. At high temperatures we observed only CuAu- and Cu_3Au-type BNSL phases (Figure 5b). When the PbSe-to-Pd NC concentration ratio was lowered to ~1:4.5, no $NaZn_{13}$-type BNSLs were observed. Instead, we observed the formation of NaCl-type BNSLs at low temperatures (Figure 5c). At intermediate and high temperatures, the NCs self-assembled into AlB_2-type and CuAu + Cu_3Au BNSLs, respectively. TEM images of different PbSe-Pd BNSL phases are shown in Figure 5d−i. Additional TEM images of BNSLs assembled at different temperatures are provided in the Supporting Information (Figures S9−S12).[53]

(93) Visser, J. *Adv. Colloid Interface Sci.* **1972**, *3*, 331–363.
(94) Hunt, N.; Jardine, R.; Bartlett, P. *Phys. Rev. E* **2000**, *62*, 900–913.

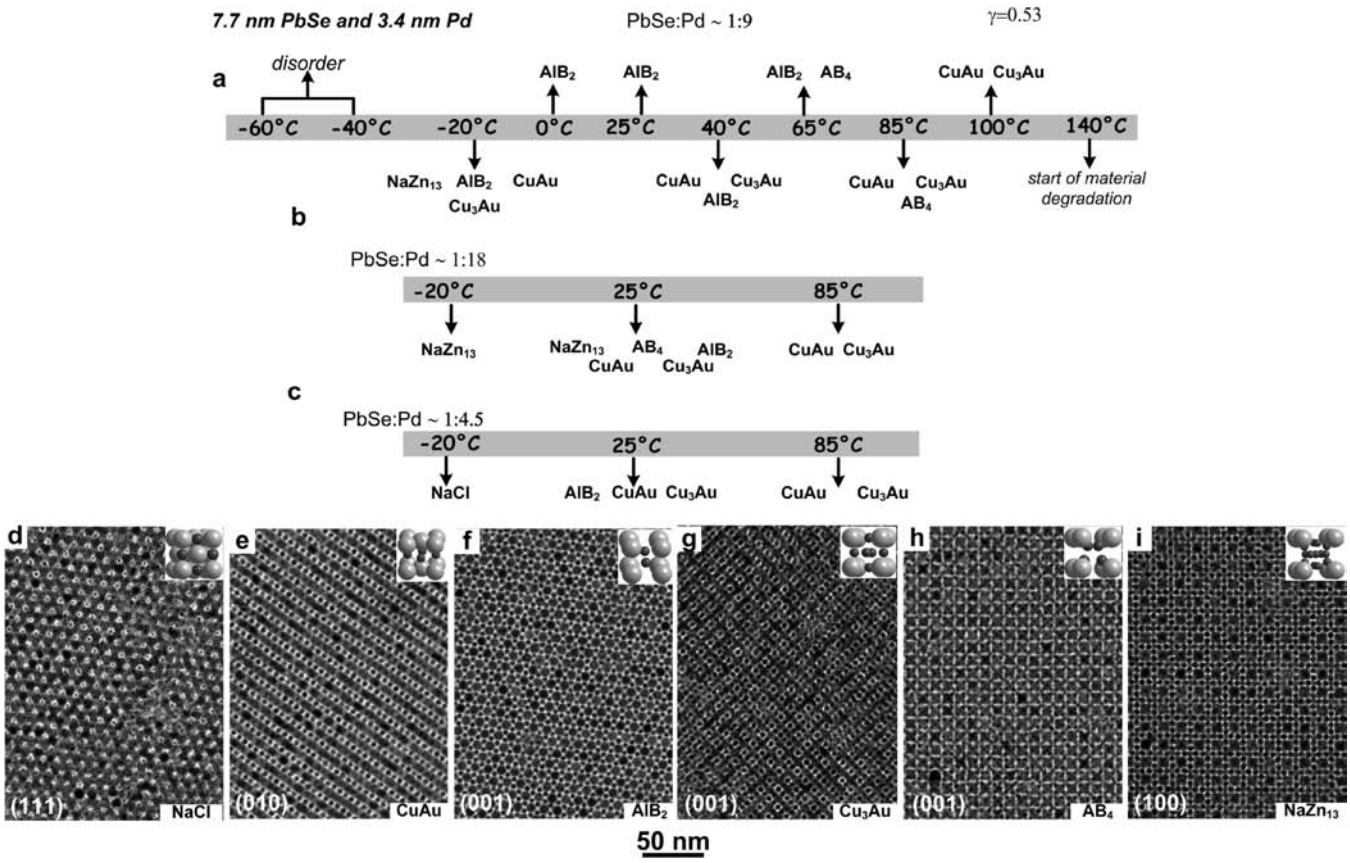

Figure 5. Effect of temperature on self-assembly of 7.7 nm PbSe and 3.4 nm Pd nanocrystals. (a−c) Overview of binary phases self-assembled at different temperatures from solutions with nanocrystal concentration ratios of (a) 1:9, (b) 1:18, and (c) 1:4.5. (d−i) TEM images of BNSLs isotructural with (d) NaCl, (e) CuAu, (f) AlB_2, (g) Cu_3Au, (h) AB_4,[53] and (i) $NaZn_{13}$ intermetallic compound.

Simultaneous formation of several BNSL phases could be either due to the existence of several binary phases with very similar chemical potentials or due to inhomogeneities in the NC samples. In addition to unavoidable size dispersion, some NCs can have small electric charge while other can be neutral.[10] Similar distribution can exist in the NC dipole moments. It is difficult to separate these effects, but the observation that, depending on the temperature, identical NC mixtures can form either only one BNSL structure or several BNSL structures (e.g., Figure 5a−c) suggests degeneration of BNSL structures at certain temperatures.

To compare the self-assembly of BNSL structures from NCs with the same chemical compositions but different γ_{eff} ratios, we synthesized 4.9 nm Pd NCs and studied their co-assembly with 7.7 nm PbSe NCs ($\gamma_{eff} \approx 0.74$). For the highest Pd-to-PbSe NC concentration ratios, we again observed the formation of $NaZn_{13}$ BNSLs at low temperatures (Figure 6a,d), despite its rather low packing density ($\rho \approx 0.61$ at $\gamma = 0.74$). This structure disappeared for lower Pd-to-PbSe NC ratios, being replaced by the $CaCu_5$-type BNSL (Figure 6b,c,h). The space-filling curve for the $CaCu_5$ lattice has a high-density branch with $\rho \approx 0.67$ at $\gamma = 0.74$ (Figure 3), which can explain the appearance of this structure at large γ. Also, contrary to the system with $\gamma = 0.53$, we observed $MgZn_2$-type Laves-phase BNSLs self-assembled at 65 °C. The packing density of the $MgZn_2$ lattice is much higher at $\gamma = 0.74$ than at $\gamma = 0.53$ (Figure 3). The CuAu and CsCl structures showed a clear domination at higher temperatures (Figure 6, Table S2), which is also consistent with their highest packing density for this γ. Figures 6d−i and S13 show typical TEM images of all BNSL structures self-assembled from 7.7 nm PbSe and 4.9 nm Pd NCs.

3.5. Analysis of the Effect of Temperature on BNSL Self-Assembly. Figures 4−6 show that different colloidal NCs self-assemble at different temperatures into distinctively different BNSL phases. The reproducible formation of different binary phases from identical NC solutions can be used as a powerful synthetic tool for directing the self-assembly process. It also provides important insight into the thermodynamics of the NC assembly process.

As discussed in section 3.2, proper selection of solvents can provide nearly temperature-independent electrostatic and vdW forces between NC cores. The interactions between hydrocarbon chains of surface ligands can be temperature-dependent, as was shown by atomistic molecular dynamics simulations by Vlugt et al.[32] At the same time, in a good solvent like *n*-alkane, direct ligand−ligand interactions are efficiently screened and become purely repulsive, providing steric stabilization to NC colloids.[32] This picture changes dramatically after solvent evaporation, which converts ligand−ligand interactions from repulsive to strongly attractive.[32,95]

Each BNSL structure has characteristic internal energy and entropy $\{U_{AB_n};S_{AB_n}\}$ per particle. The relative weights of internal energy and entropy scale according to eq 1. With increasing temperature, the role of S_{AB_n} increases, and BNSLs with larger entropic components should become more stable compared to the structures stabilized by interparticle interactions. Since the

(95) Mueggenburg, K. E.; Lin, X.-M.; Goldsmith, R. H.; Jaeger, H. M. *Nat. Mater.* **2007**, *6*, 656–660.

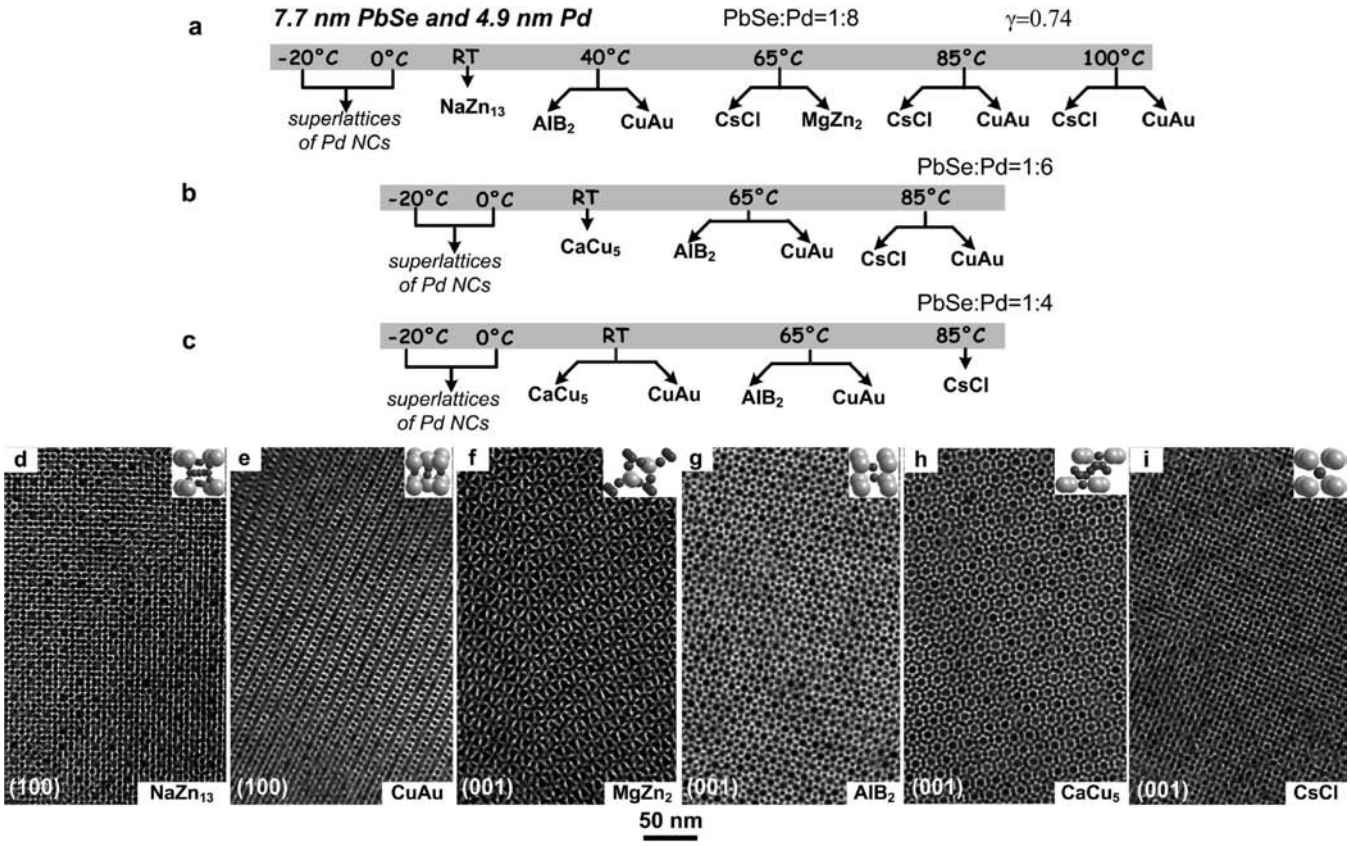

Figure 6. Self-assembly of 7.7 nm PbSe and 4.9 nm Pd nanocrystals at different temperatures. (a−c) Schematic illustration of binary phases assembled at different temperatures from solutions with different nanocrystal concentration ratios. (d−h) TEM images of BNSLs isostructural with (d) $NaZn_{13}$, (e) CuAu, (f) $MgZn_2$, (g) AlB_2, (h) $CaCu_5$, and (i) CsCl structures.

free volume entropy is approximately proportional to ρ, it is reasonable to expect that high-temperature phases should also have the highest packing density for a given γ ratio.

In an 8 nm CdSe−3.1 nm PbS NC system ($\gamma_{eff} \approx 0.47$), the temperature-driven transition from the low-density $NaZn_{13}$-type BNSLs to the high-density AlB_2 and NaCl structures (Figure 4) follows this expected trend. We could not find calculated phase diagrams for hard-sphere mixtures at $\gamma = 0.47$, but the calculations by Trizac et al. for the close case of $\gamma = 0.45$ predict that both NaCl and AlB_2 binary structures can form from hard spheres at this γ.[36] The mixture of hard spheres with the concentration ratio of large to small spheres $n_L:n_S = 1:8$ should undergo the following sequence of phase transitions upon gradual increase of the particle concentration:[36]

$$\mathrm{F} \overset{\mathrm{I}}{\Rightarrow} (\mathrm{AlB_2} + \mathrm{F}) \overset{\mathrm{II}}{\Rightarrow} (\mathrm{AlB_2} + \mathrm{S} + \mathrm{F}) \overset{\mathrm{III}}{\Rightarrow} (\mathrm{AlB_2} + \mathrm{S}) \overset{\mathrm{IV}}{\Rightarrow} (\mathrm{AlB_2} + \mathrm{NaCl} + \mathrm{S}) \overset{\mathrm{V}}{\Rightarrow} (\mathrm{NaCl} + \mathrm{S}) \quad (6)$$

where F and S stand for the fluid (disordered phase) and the fcc lattice of small particles, respectively. The AlB_2 phase should form first during solvent evaporation. In a hard-sphere system this binary phase converts to the NaCl-type lattice when the particle volume fraction exceeds ~0.65. In real NCs, the presence of attractive vdW forces can destabilize NC solutions before approaching this volume fraction and "freeze" the NCs in the AlB_2 phase, which probably occurs at 0−40 °C. It is known that the solubility of NCs capped with hydrocarbon surface ligands increases with temperature. We may then explain the formation of the NaCl phase at high temperatures on the basis of increasing the colloidal stability of NC solutions up to the concentrations required for the $AlB_2 \rightarrow$NaCl phase transition (transitions IV and V in eq 6).

Eldridge et al. calculated the range of stability for $NaZn_{13}$ structures in hard-sphere mixtures as $0.474 \leq \gamma \leq 0.626$.[25] γ_{eff} of our CdSe-PbS NCs is very close to the lower boundary of this stability range, and formation of $NaZn_{13}$-type BNSLs is not totally unexpected. Moreover, the finite size distributions of CdSe and PbS NCs can create sub-ensembles of NCs with γ_{eff} values sufficient to entropically stabilize the $NaZn_{13}$ lattice. These arguments, however, cannot explain why we did not observe any other BNSL structures at low temperature and did not observe $NaZn_{13}$ BNSLs at higher temperatures. The most plausible explanation is that the cohesive energy of $NaZn_{13}$ BNSLs is higher compared to those of AlB_2 and NaCl BNSLs and of close-packed PbS NCs. The internal energy term then rivals free volume entropy at low temperatures but is not sufficient to dominate over the $-T\Delta S$ term at high temperatures. The possible reasons for energetic stabilization of $NaZn_{13}$ BNSLs will be discussed later.

Self-assembly of PbSe and Pd NCs (Figures 5 and 6) resulted in a significantly richer palette of binary phases compared to the CdSe-PbS system. We attribute this to strong vdW interactions between Pd NCs, which increased the total weight and complexity of energetic contributions to the free energy of self-assembly. BNSLs self-assembled from mixtures of 7.7 nm PbSe and 3.4 nm Pd NCs ($\gamma_{eff} \approx 0.53$) included both the binary phases expected for hard spheres ($NaZn_{13}$, AlB_2, NaCl) and a number of low-density phases, such as CuAu, Cu_3Au, and the AB_4 lattice shown in Figure S4. The phase diagrams calculated for binary

hard-sphere mixtures at $\gamma = 0.54$ predicted formation of AlB_2 and $NaZn_{13}$ binary phases,[94] which was verified in the experimental studies by Hunt et al. on sterically stabilized PMMA spheres with $\gamma = 0.52$.[94] The behavior of PbSe and Pd NCs revealed stark disagreement with both theory and the experiments on PMMA spheres. Instead of two binary phases assembled from PMMA spheres, the NCs formed at least six binary phases. At low temperatures (−20 to 25 °C) we observed $NaZn_{13}$ BNSLs when Pd NCs were present in a large excess compared to PbSe NCs (Figure 5a,b,i). At low PbSe-to-Pd NC ratios, NaCl-type was the sole low-temperature BNSL phase (Figure 5c,d). At high temperatures CuAu and Cu_3Au were the dominant BNSL phases (Figure 5e,g). These structures have $\rho \approx 0.60$ at $\gamma = 0.53$, which is much lower than the density of AlB_2 packing. Our study clearly showed that co-assembly of 7.7 nm PbSe and 3.4 nm Pd NCs cannot be explained by entropy-driven crystallization. Instead, self-assembly of these NCs should be primarily driven by interparticle interactions.

To further explore the driving forces responsible for self-assembly of PbSe and Pd NCs, we combined 7.7 nm PbSe with 4.9 nm Pd NCs ($\gamma_{eff} \approx 0.74$). In hard-sphere calculations, this γ ratio is known to form no thermodynamically stable binary phases,[87,94] which was also confirmed in experimental studies on PMMA particles.[94] In contrast to these predictions, PbSe and Pd NCs formed six different BNSL phases (Figure 6d−i). The low-density $NaZn_{13}$ ($\rho \approx 0.61$) BNSL was the low-temperature phase. The CuAu and CsCl BNSLs were assembled at high temperatures, which is also in agreement with their highest ρ values among all BNSLs self-assembled from 7.7 nm PbSe with 4.9 nm Pd NCs. Comparison of BNSL phases formed between PbSe and Pd NCs at different γ shows that the space-filling principles are not totally ignored in these BNSLs. For example, $CaCu_5$ structure was observed at $\gamma = 0.74$ and not observed at $\gamma = 0.53$, in agreement with its higher packing density at large γ ($\rho \approx 0.67$ vs 0.59 for the above γ ratios, respectively). The same applies to the $MnZn_2$ BNSL, with ρ approaching reasonably high values only at large γ ratios (Figure 3).

The observed difference in the self-assembly behavior of CdSe-PbS and PbSe-Pd NCs outlines the general complexity principle in BNSL structures. Since the Hamaker constants for both CdSe and PbS phases interacting through a layer of hydrocarbon ligands are comparable, the vdW contribution to the free energy should scale approximately with the lattice packing density, and simple hard-sphere packing models should reasonably accurately describe behaviors of real NCs. On the other hand, if there is a large difference in interaction energies between large and small NCs (e.g., in BNSLs combining semiconductor and metal NCs), BNSL phase diagrams gain complexity, leading to non-compact phases and even truly complex binary structures such as Archimedean tailings and quasicrystals.[22]

An important general observation which can be derived from our experimental data is that, in all three studied systems, $NaZn_{13}$ BNSLs formed exclusively at low temperatures. We can propose two possible explanations for such behavior. First, the assembly of AB_{13}-type lattice can be largely driven by the ΔU in eq 1 rather than by the free volume entropy. The second possibility is related to the kinetics of NC assembly. The assembly pathway for $NaZn_{13}$ lattices could involve pre-assembly of icosahedral clusters of Pd NCs in solution driven by vdW and electrostatic forces, followed by the integration of these clusters into growing $NaZn_{13}$ lattices (Figure S14). Such cluster assembly has been anticipated in recent theoretical studies[96] and requires a delicate competition between attractive potentials and k_BT.

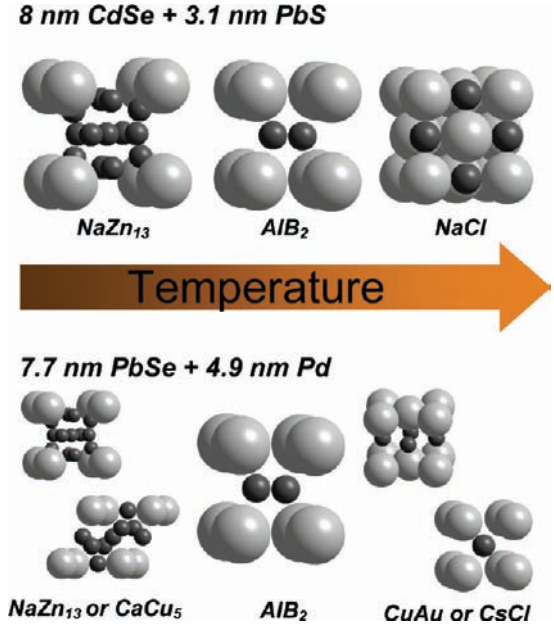

Figure 7. Unit cells of binary nanoparticle superlattices self-assembled at different temperatures. See text for discussion of BNSL structural evolution caused by energetic and entropic contributions to the free energy of self-assembly.

Another interesting trend observed in all three NC systems is schematically outlined in Figure 7. The low-temperature BNSL phases ($NaZn_{13}$ and $CaCu_5$) comprised a sub-lattice of large NCs separated by clusters of small NCs. In the $NaZn_{13}$ lattice these clusters include 13 NCs. The clustering in the $CaCu_5$ lattice is less evident, but the structure can be deconvoluted into a simple hexagonal packing of large spheres and close-packed trigonal bipyramidal clusters of five small spheres. The AlB_2 lattice typically observed at intermediate temperatures contains "clusters" of two small NCs (Figure 7). All high-temperature BNSL structures (NaCl, CuAu, CsCl, and Cu_3Au) have no touching small spheres. If small NCs exhibit stronger attractive forces than large NCs, the binary lattices incorporating "clusters" of small NCs should gain additional stability from short-range attraction between tightly packed small NCs. This should be especially evident in the PbSe-Pd system because of strong vdW interactions between Pd NCs.

Formation of many BNSL phases in a relatively small temperature window requires that $|\Delta U|$ and $|\Delta TS|$ in eq 1 should be of the same order of magnitude, with $|\Delta U| < |\Delta TS|$ during assembly of CdSe-PbS NCs and $|\Delta U| > |\Delta TS|$ for PbSe-Pd NCs. The driving force of NC self-assembly gradually shifts from the interparticle interactions (low-T limit) to free-volume entropy (high-T limit), leading to $NaZn_{13}$ BNSLs at low temperatures, whereas the high-temperature structures should be those with the largest ρ for each γ ratio.

4. Conclusions

We have shown that temperature can be used as a convenient tool for directing self-assembly of NCs into different single-component and binary structures. A comparison of calculated hard-sphere phase diagrams with our experimental studies of

(96) Keys, A. S.; Glotzer, S. C. *Phys. Rev. Lett.* **2007**, *99*, 235503.

NC assembly revealed significantly richer behavior of NCs compared to the non-interacting spherical particles. In the absence of strong electrostatic interactions and vdW forces, as, e.g., in the CdSe+PbS BNSLs, hard-sphere phase diagrams correlated well with the behaviors of real NCs at high temperatures. On the other hand, self-assembly of BNSLs including metal NCs (e.g., PbSe+Pd) cannot be rationalized using hard-sphere models because of strong interparticle interactions. Contrary to the case of CdSe-PbS NCs, entropy seems to play only a limited role in the stabilization of PbSe-Pd BNSLs. The observed structural diversity of BNSLs is a result of comparable contributions of entropy-driven crystallization and interparticle interactions, with the possibility of adjusting energetic and entopic contributions through chemical design of NCs and with many complex binary phases formed under appropriate experimental conditions.

Acknowledgment. We thank E. V. Shevchenko (Argonne National Laboratory), A. Moore and T. Witten (University of Chicago) for stimulating discussions, and S. M. Rupich (University of Chicago) for synthesis of PbS and PbSe nanocrystals. The work was supported by the NSF MRSEC Program under Award No. DMR-0213745 and by the David and Lucile Packard Foundation. M. I. B. and W. H. acknowledge financial support from the Austrian Nanoinitiative (NSI). The work at the Center for Nanoscale Materials (ANL) was supported by the U.S Department of Energy under Contract No. DE-AC02-06CH11357.

Supporting Information Available: Additional experimental and calculation details; structural characterization of BNSLs using electron diffraction (Figure S1) and TEM tilting studies (Figures S2−S4); TEM images for close-packed and non-close-packed superlattices of $Fe_xO/CoFe_2O_4$ NCs (Figures S5−S7); electrophoretic mobility measurements for colloidal NCs used in self-assembly experiments (Figure S8); calculation details for space-filling curves; additional TEM images of BNSLs self-assembled from PbSe and Pd NCs (Figures S9−S13); summary of surface area coverage by different binary superlattice structures (Tables S1 and S2); pathway for self-assembly of BNSL structures with complex unit cells incorporating clusters of metal NCs (Figure S14). This material is available free of charge via the Internet at http://pubs.acs.org.

JA103083Q